

# 1 Storylines of Summer Arctic climate change constrained by Barents-Kara Sea and 2 Arctic tropospheric warming for climate risks assessment

3 Xavier J. Levine<sup>1</sup>, Ryan S. Williams<sup>2</sup>, Gareth Marshall<sup>2</sup>, Andrew Orr<sup>2</sup>, Lise Seland Graff<sup>3</sup>, Dörthe  
4 Handorf<sup>4</sup>, Alexey Karpechko<sup>5</sup>, Raphael Köhler<sup>4</sup>, René Wijngaard<sup>6</sup>, Nadine Johnston<sup>2</sup>, Hanna Lee<sup>7,1</sup>, Lars  
5 Nieradzick<sup>8</sup>, Priscilla A. Mooney<sup>1</sup>

6 <sup>1</sup>Norwegian Research Centre, 5004 Bergen, Norway

7 <sup>2</sup>British Antarctic Survey, CB3 0ET Cambridge, United Kingdom

8 <sup>3</sup>Norwegian Meteorological Institute, 0371 Oslo, Norway

9 <sup>4</sup>Alfred Wegener Institute, 14473 Potsdam, Germany

10 <sup>5</sup>Finnish Meteorological Institute, FI-00560 Helsinki, Finland

11 <sup>6</sup>Utrecht University, 3584 CS Utrecht, The Netherlands

12 <sup>7</sup>Norwegian University of Science and Technology, 7491 Trondheim, Norway

13 <sup>8</sup>Lund University, 221 00 Lund, Sweden

14 *Correspondence to:* Xavier J. Levine ([xale@norceresearch.no](mailto:xale@norceresearch.no))

## 15 Abstract

16  
17 While climate models broadly agree on the changes expected to occur over the Arctic with global warming on a pan-Arctic  
18 scale (i.e., polar amplification, sea-ice loss, increased precipitation), the magnitude and patterns of those changes at regional  
19 and local scales remain uncertain. This limits the usability of climate model projections for risk assessments and their impact  
20 on human activities or ecosystems (e.g., fires, permafrost thawing). Whereas any single or ensemble-mean projection may be  
21 of limited use to stakeholders, recent studies have shown the value of the storyline approach in providing a comprehensive and  
22 tractable set of climate projections that can be used to evaluate changes in environmental or societal risks associated with  
23 global warming.

24 Here, we apply the storyline approach to a large ensemble of CMIP6 models, with the aim of distilling the wide spread in  
25 model predictions into four physically plausible outcomes of Arctic summertime climate change. This is made possible by  
26 leveraging strong covariability in the climate system, associated with well-known but poorly constrained teleconnections and  
27 local processes: specifically, we find that differences in Barents-Kara Sea warming and lower tropospheric warming over polar  
28 land regions among CMIP6 models explain most of the inter-model variability in pan-Arctic surface summer climate response  
29 to global warming. Based on this novel finding, we compare regional disparities in climate change across the four storylines.  
30 Our storyline analysis highlights the fact that, for a given amount of global warming, certain climate risks can be intensified  
31 while others may be lessened, relative to a “middle-of-the-road” ensemble mean projection. We find this to be particularly  
32 relevant when comparing climate change over terrestrial and marine areas of the Arctic, which can show substantial differences



33 in their sensitivity to global warming. We conclude by discussing potential implications of our findings for modelling climate  
34 change impacts on ecosystems and human activities.

## 35 **1 Introduction**

36 Since the late twentieth century, the surface of the Arctic has warmed 2 to 4 times greater than the global average, which is  
37 referred to as Arctic amplification (hereinafter AA, e.g., Jansen et al., 2020; England et al., 2021; Rantanen et al., 2022). This  
38 warming amplification of the near-surface and troposphere is caused by a number of feedbacks involving oceanic, cryospheric  
39 and atmospheric processes (Previdi et al., 2021). In particular, sea-ice cover loss in the Arctic Ocean explains the bulk of the  
40 near-surface warming, especially over marine areas and coastal terrestrial regions due to its impact on surface energy fluxes  
41 and upper ocean warming (e.g., Screen and Simonds, 2010; Dai et al., 2019; Jenkins and Dai, 2021). Sea-ice loss and sea  
42 surface warming have been singularly strong in the Barents-Kara Sea, which has been identified as a warming hotspot (Lind  
43 et al. 2018) and a mediator of climate change between the North Atlantic and Central Arctic Oceans (Smedsrud et al., 2013).  
44 AA is also tied to tropospheric warming, which is influenced to a greater extent by atmospheric dynamical feedback, such as  
45 temperature feedbacks (Pithan and Mauritsen, 2014) and poleward atmospheric energy transport feedback (e.g., Merlis and  
46 Henry, 2018). Overall, the combined influence of oceanic, cryospheric and atmospheric processes render Arctic climate change  
47 and its surface warming amplification particularly complex to predict.

48  
49 AA has resulted in extensive loss of land ice, snow cover, and thawing of the permafrost over the Arctic region (e.g., Callaghan  
50 et al., 2011; van den Broeke et al., 2016; Chadburn et al., 2017; Shepherd and IMBIE Team, 2020). These profound changes  
51 to the Arctic climate system have been linked to increases in a range of societal and ecological risks (Yumashev et al., 2019).  
52 For example, the past decades have shown an increase in the frequency and intensity of wildfires in many Arctic regions, such  
53 as North America's boreal forests (Masrur et al., 2018; McCarty et al., 2021), which has been attributed to unusually warm  
54 and dry spring and summer weather conditions (Krikken et al., 2019), as well as increased lightning activity (Veraverbeke et  
55 al., 2017). Likewise, the accelerated thawing of permafrost over large swathes of the terrestrial Arctic poses significant  
56 challenges for the integrity of local infrastructure, such as roads and buildings (Hjort et al., 2022). Impacts of climate change  
57 in the Arctic also extend to marine areas. For example, while increased sunlight in the photic zone from sea-ice loss and warmer  
58 sea surface temperature may have boosted marine primary production in the Arctic oceans in past decades (Arrigo and Van  
59 Dijken, 2015), evidence suggests that this is primarily benefiting species typically found at lower latitudes at the expense of  
60 the native Arctic species (Ingvaldsen et al., 2021). The changes to the Arctic climate system also have profound impacts beyond  
61 this region, including causing increases in extreme weather over the Northern Hemisphere mid-latitudes (Cohen et al., 2014).  
62 The loss of glaciers / land ice from Greenland through both increased surface meltwater runoff and increased glacier flow /  
63 dynamic ice loss has been a major contributor to increased global sea-level rise (e.g., Rignot et al., 2011; Shepard and IMBIE  
64 team, 2020).



65  
66 Assessing the many impacts of climate change in the Arctic requires a strong understanding of the physical state of the  
67 atmosphere, ocean, and sea ice, and how it will respond to climate change. This, however, has been hampered by future climate  
68 projections from global coupled climate models showing a wide range of possible outcomes (Overland et al., 2019; Notz et  
69 al., 2020; McCrystall et al., 2021; IPCC, 2021), which stems from uncertainties in possible future greenhouse gas emission  
70 scenarios, an incomplete understanding of key climate processes and an imperfect representation of them in the models (model  
71 uncertainty), and natural (internal) variability within the climate system (Hawkins and Sutton, 2009). This lack of certainty  
72 poses considerable challenges for planning effective mitigation strategies by stakeholders impacted locally or remotely by  
73 Arctic climate change. The issue is often poorly addressed through the use of either a single-model or multi-model mean  
74 climate projection (Shepherd et al., 2018).

75  
76 The storyline approach overcomes the limitations of the above approaches by identifying and describing physically plausible  
77 and self-consistent pathways that are representative of future climate change, which may be more helpful to develop mitigation  
78 strategies (Shepherd et al., 2018). Those storylines express the response of the Arctic climate to global warming conditional  
79 on a range of environmental conditions being realised. They are based on a methodology recently developed for studying the  
80 impact of climate change in other areas, primarily in the midlatitudes, e.g., western and central Europe (Zappa and Shepherd,  
81 2017 [ZS17]) or Southern Hemisphere midlatitude regions (Mindlin et al., 2020 [M20]). In this study, we posit that a substantial  
82 fraction of the variability of the surface climate response to global warming in the Arctic is associated with the warming of the  
83 Barents-Kara Sea and the warming of the Arctic lower troposphere. This is borne out of Barents-Kara Sea warming and the  
84 lower tropospheric warming being strongly influenced by climate variability at lower latitudes, but also being key players in  
85 driving surface warming in the Arctic. The Barents-Kara Sea, while being sensitive to changes in the Atlantic storm track  
86 (Jung et al., 2017) and the tropics (Warner et al., 2020), have long been recognised as a key modulators of climate variability  
87 in Earth's Northernmost regions (Li et al., 2020; Peings et al., 2023). Likewise, the warming of the Arctic lower troposphere,  
88 which is sensitive to changes in poleward atmospheric heat transport from lower latitudes (Russotto and Biasutti, 2020),  
89 strongly influences the near-surface climate through its impact on the boundary layer stability and surface radiative forcing  
90 (e.g., Previdi et al., 2020).

91  
92 Using a range of possible scenarios for the Barents-Kara Sea and Arctic lower tropospheric warming that emerge from climate  
93 model simulations, we devise storylines of future climate change for the Arctic regions. Specifically, we compare the climate  
94 of the last 30-years of the 21st century (2070–2099) projected in a high-end global warming scenario (corresponding with 8.5  
95  $W m^{-2}$  additional increase in radiative forcing by 2100 relative to preindustrial, the Shared Socioeconomic Pathways 5-8.5,  
96 SSP5-8.5; see O'Neill et al. 2016 and Meinshausen et al., 2020), with the last 30 years of the historical experiment (1985–  
97 2014). SSP5-8.5 represents the upper boundary of the range of scenarios described in ScenarioMIP and is useful to obtain the  
98 strongest possible response to climate change within the framework of the CMIP6; this ensures that the impact of internal



99 climate variabilities is minimised in our study. We focus on the summer season, due to its relevance to societal and ecological  
100 impacts at high-latitude that peak in the warm part of the year, such as, among others, high-latitude fires, trans-Arctic shipping,  
101 and marine primary production. After describing the dataset and methodology used for our storyline analysis in section 2, we  
102 describe in section 3 how our Arctic storylines differ from the multi-model ensemble mean response, as established by four  
103 target variables we identified as being most relevant for studying climatic impacts in the region. We discuss the relevance of  
104 our findings for evaluating climate impacts in the Arctic region in section 4.

## 105 **2 Data and Methodology**

### 106 **2.1 Model data**

107 Our analysis uses a set of 42 climate models from CMIP6, which we downloaded from The Earth System Grid Federation  
108 (ESGF; Cinquini et al., 2014; models with members are listed on Table 1). The model and number of ensemble members  
109 (given in parentheses) include: TaiESM1 (1), BCC-CMS2-MR (1), CAS-ESM2-0 (2), FGOALS-f3-L (1), IITM-ESM (1),  
110 CanESM5 (15), CanESM5-CanOE (3), CMCC-CM2-SR5 (1), CMCC-ESM2 (1), CNRM-CM6-1 (6), CNRM-ESM2-1 (5),  
111 ACCESS-ESM1-5 (15), ACCESS-CM2 (5), E3SM-1-0 (5), E3SM-1-1 (1), E3SM-1-1-ECA (1), EC-Earth3 (15), EC-Earth3-  
112 CC (1), EC-Earth3-Veg-LR (3), FIO-ESM-2-0 (3), INM-CM4-8 (1), INM-CM5-0 (1), IPSL-CM6-LR (7), MIROC-ES2L (10),  
113 MIROC6 (15), HadGEM3-GC31-LL (4), HadGEM3-GC31-MM (4), UKESM1-0-LL (5), MPI-ESM1-2-LR (15), MRI-  
114 ESM2-0 (6), GISS-E2-1-G (14), GISS-E2-1-H (10), CESM2 (3), CESM2-WACCM (3), NorESM2-LM (1), NorESM2-MM  
115 (1), KACE-1-0-G (3), GFDL-CM4 (1), GFDL-ESM4 (1), NESM3 (2), CIESM (1), MCM-UA-1-0 (1). For each model, all  
116 ensemble members of the historical experiment that were extended into the SSP5-8.5 scenario are used, capped to a maximum  
117 of 15 members per model. For each model, we produce a mean climatology of the ensemble members for both the historical  
118 and SSP5-8.5 experiment, in their respective period of evaluation (i.e., 1985-2014 and 2070-2099), to reduce the weight of  
119 internal variability in the climate projections. Therefore, every model is represented by one climate projection regardless of  
120 their number of members, whether it is a single member or an ensemble-mean of members. As most models only have a few  
121 members, setting a maximum of 15 members seems a reasonable trade-off for reducing internal variability while limiting  
122 computational resources needed to produce ensemble means for the few models that have many members.

### 123 **2.2 Multivariate Linear Regression Analysis**

124 The climate storyline approach is based on a multivariate linear regression (MLR) analysis that expresses the response to  
125 global warming of any variable,  $Z$  (“target variable”), as a linear superposition of its response to changes in  $N$  climate indices,  
126  $P_i$ , (“predictor index”). Following the methodology outlined in Zappa and Shepherd (2017), this can be expressed as:

$$128 \Delta Z(x, m) = \overline{\Delta Z}(x) + \sum_{i=1}^N \beta_i(x) \widehat{\Delta P}_i(m) \quad (1a)$$



129 where  $\Delta\widehat{P}_i(m) = \Delta P_i(m) - \overline{\Delta P}_i$  (1b)

130 Here,  $\Delta Z$  defines changes in target variable  $Z$ ,  $\Delta P_i$  changes in predictor index  $P_i$ , and  $\beta_i$  is the response of variable  $Z$  to changes  
 131 in  $P_i$ . Note that the target variable  $Z$  varies both in space  $[x]$  and across models  $[m]$ , but predictor indices  $P_i$  only vary across  
 132 models; predictor indices are typically regional averages of variables that are tied to well-known physical features of the  
 133 climate.  $\overline{(\cdot)}$  defines a multi-model ensemble mean (MMM) and  $\widehat{(\cdot)}$  a deviation from the MMM;  $\Delta$  defines the difference in  
 134 climatology between the 2070–2099 (SSP5-8.5 emission scenario) and 1985–2014 (historical experiment) period, normalised  
 135 by a global warming index,  $(T_{ssp585} - T_{hist})$ , i.e.,

$$136 \quad \Delta X = \frac{(X_{SSP585} - X_{hist})}{(T_{SSP585} - T_{hist})} \quad (2)$$

137 Here,  $T$  is the annual global-mean 2 m temperature, and  $X$  defines any target variable or predictor index. Normalisation ensures  
 138 that changes in target variables and predictor indices are not directly associated with changes in the global warming index  
 139 ( $GWI$ , with  $GWI = T_{SSP585} - T_{hist}$ ). Instead, the normalised response describes the variability in target variables or predictor  
 140 indices linked to the underlying changes in the dynamics of the atmosphere/ocean/ice triggered by global warming, rather than  
 141 the variability directly affected by the model's climate sensitivity.

142

143 Storylines are constructed using the coefficients  $\beta_i$  emerging from the MLR analysis (Eq. 1), which are compounded with a  
 144 standardised climate response for each predictor. In a 2-predictors MLR analysis, this amounts to the creation of 4 storylines  
 145 that are representative of the diversity in the climate change response across CMIP6 models:

146

$$147 \quad \text{A. } \widehat{\Delta Z}_{-,+}(x) = s (-\beta_1(x) + \beta_2(x)) \gamma, \quad (3a)$$

$$148 \quad \text{B. } \widehat{\Delta Z}_{+,+}(x) = s (+\beta_1(x) + \beta_2(x)) \Gamma, \quad (3b)$$

$$149 \quad \text{C. } \widehat{\Delta Z}_{-,-}(x) = s (-\beta_1(x) - \beta_2(x)) \Gamma, \quad (3c)$$

$$150 \quad \text{D. } \widehat{\Delta Z}_{+,-}(x) = s (+\beta_1(x) - \beta_2(x)) \gamma, \quad (3d)$$

$$151 \quad \text{where } \Gamma = \frac{1}{2} \frac{1-r^2}{1-r} \text{ and } \gamma = \frac{1}{2} \frac{1-r^2}{1+r}. \quad (3e)$$

152 Here,  $s$  defines the standardised climate response, whose value is set to 1.26. This value is derived from a Chi-square  
 153 distribution for 2 degrees of freedom and evaluated on the edge of the 80% confidence boundary region; this distribution is  
 154 applied to the standardised intermodel spread in our 2 predictors from the large ensemble of CMIP6 simulations described in  
 155 section 2.1. In simpler terms,  $s$  defines a standardised deviation from the MMM of equal magnitude in our 2 predictor indices,  
 156 which we deem plausible and yet not so extreme to be unlikely, based on the projection spread across CMIP6 simulations. To  
 157 account for a weak positive correlation between both predictor indices, the storylines in Eq. (3) also contain factors  $\Gamma$  and  $\gamma$ ,  
 158 which depends on the correlation coefficient  $r$  (see M20 for more details).

159



160 The MLR framework of Eq. (1) and (3) seeks to predict the inter-model variability in the projections, and not the multi-model  
161 ensemble mean climate response; this is borne out of our storylines' aim, that is to explore a range of possible climate  
162 realisations representative of the diversity in model projections. While the MLR framework is compatible with using any  
163 number of predictor indices, the exponential increase in storylines with the number of predictors ( $2^N$  storylines can be produced  
164 for a set of  $N$  predictors) prompts us to use as few predictors as necessary, to keep the number of storylines tractable. We limit  
165 ourselves to two predictors and four storylines, as our analysis demonstrates that this configuration can explain most of the  
166 intermodel spread in the warming response of the Arctic (Table 1).

### 167 **2.3 Choice of target variables**

168 Due to their relevance to a broad array of climate risks, we select 2 m temperature, precipitation rate, 850 hPa zonal wind, and  
169 sea-ice fraction as target variables for understanding the impact of Arctic climate change (Lee et al., 2002). Note that the 850  
170 hPa zonal wind is considered to be a good proxy of the near-surface wind while being less sensitive to the physical  
171 parameterization of surface processes (e.g., ZS17). This choice of variables is highly relevant to many key climate-driven risks  
172 in the Arctic, including wildfires, permafrost thawing, sea-ice loss, and marine heatwaves (Anisimov and Nelson, 1997; Pabi  
173 et al., 2008; Arrigo and Van Dijken, 2015; Melia et al., 2016). For instance, Arctic wildfires are sensitive to warm, dry, and  
174 windy conditions, which implies a dependence on near-surface air temperature, near-surface wind, and precipitation accrued  
175 during the warm season (Dowdy et al., 2010). We define 2 m temperature as our reference target variable because of its  
176 preponderance in driving those climate risks. This means that our storylines are optimised to represent the variability in the 2  
177 m temperature.

### 178 **2.4 Choice of predictor indices**

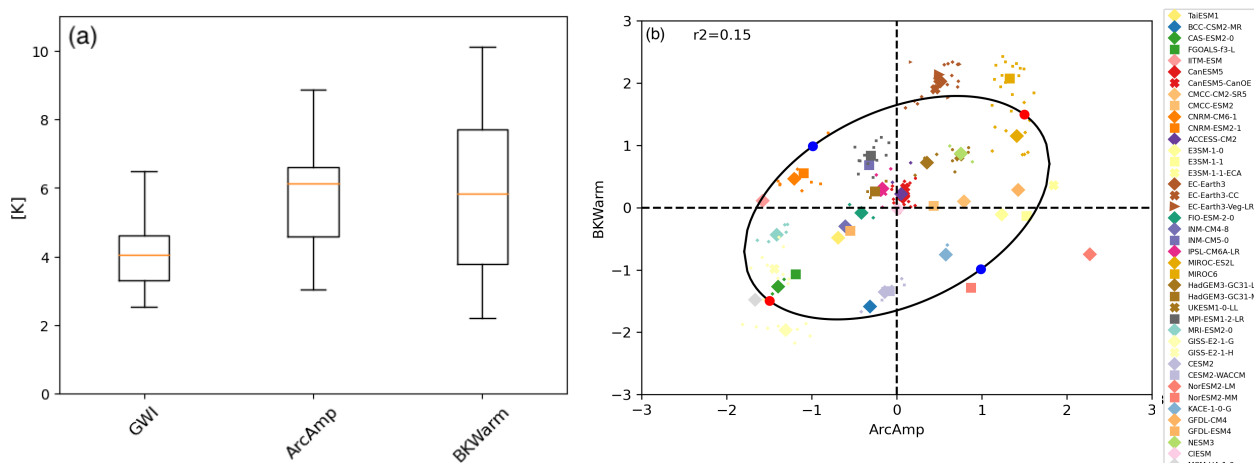
179 Using the MLR approach the target variables' response to global warming may be regressed upon the two climate indices that  
180 we consider optimal for explaining differences in climate change projections between the CMIP6 model simulations. In this  
181 study, we select Arctic atmospheric amplification and Barents-Kara Sea warming as our predictors, which we refer to  
182 respectively as 'ArcAmp' and 'BKWarm'. ArcAmp is defined as the 850 hPa temperature change averaged over all areas  
183 poleward of  $55^\circ$  N, and BKWarm as the sea-surface temperature change averaged over the Barents-Kara Sea (its outline is  
184 shown on Fig. 2). Both 'ArcAmp' and 'BKWarm' are defined over the extended summer season (May to October). As  
185 explained below, we choose those two predictors owing to (i) their ability to explain a large fraction of the inter-model  
186 variability in climate change projections, and to (ii) their connection to a wide array of climatic phenomena in the Arctic and  
187 in midlatitude regions, especially near-surface warming.



188 **3 Results**

189 Figure (1a) shows the intermodel spread in ArcAmp, BKWarm and GWI, which is of comparable magnitude to their MMM  
 190 value for all three indices; yet we note that the spread is larger for ArcAmp and BKWarm than GWI. This large spread reflects  
 191 known uncertainties in the warming of the Barents-Kara Sea and the lower Arctic troposphere in climate models, which are  
 192 associated with poorly constrained physical processes and teleconnections influencing the Arctic climate (e.g., Previdi et al.,  
 193 2021). Figure (1b) shows ArcAmp and BKWarm for all CMIP6 models, which shows a weak correlation in their values ( $r^2 =$   
 194 0.15); this is made evident by the elliptically shaped confidence boundary region on Fig. 1b, which accounts for the larger  
 195 spread in variance along the direction of correlation (the ellipticity is determined by the  $\Gamma$  and  $\gamma$  factors in Eq. 3). This nearly  
 196 satisfies an important condition of orthogonality necessary for the effective combined use of ArcAmp and BKWarm as  
 197 predictors in the MLR framework (Eq. 1). The independence in the changes of ArcAmp and BKWarm suggests that the  
 198 sensitivity of the Barents-Kara Sea and that of the lower troposphere (850 hPa) to global warming are controlled by different  
 199 physical processes--even if changes in both predictor indices are ultimately driven by global warming.

200



201

202 **Figure 1: (a)** Boxplot showing the Global Warming Index (GWI), and the two predictor indices used for the storylines (ArcAmp and  
 203 BKWarm). GWI is defined as the global and annual-mean response of the 2 m temperature, ArcAmp the response of the 850 hPa  
 204 temperature averaged over all regions poleward of 55° N, and BKWarm the response of the sea surface temperature averaged over  
 205 the Barents-Kara Sea (units: K). Both ArcAmp and BKWarm are defined for the extended summer season (May to October).  
 206 Response is defined as the climatological-mean difference of the last 30 years of the current century (2070-2099) with that of the  
 207 historical period (1985-2014). The lowest and highest values are shown at the extremities of each box; box delimiters define the 25<sup>th</sup>  
 208 and 75<sup>th</sup> percentiles, while the median value (50<sup>th</sup> percentile) is shown by an orange line. (b) ArcAmp and BKWarm normalised by  
 209 the GWI and with the MMM value removed for each model. Note that each predictor index is rescaled by its standard deviation,  
 210 and thus non-dimensionalised (e.g., a value of 1 means a difference of one-standard deviation from the MMM value). The solid  
 211 ellipse delimits the 80% confidence region of the model response in ArcAmp and BKWarm (Eq. 3). Dots on the ellipse show the 4  
 212 storylines defined in Eq. (3a-d).



213  
214  
215  
216  
217  
218  
219  
220  
221  
222

Applying the 2-predictors MLR framework described in Eq. (1), we find that the inter-model variance in the 2 m temperature explained by ArcAmp and BKWarm describes more than half of its overall inter-model variance (54%, see Table 1). This is close to the theoretical maximum that can be explained using a 2-predictors MLR (62%), which we evaluated as the variance explained by the first two components of a principal component analysis (PCA) applied on the normalised change in 2 m temperature (Table 1). Applying the same framework to explain changes in the 850 hPa zonal wind, precipitation rate, and sea-ice fraction, we find that the amount of variance explained by our 2-predictors MLR is substantially lower (~20%) for these variables, even if it is not insignificant. This highlights the fact that our storylines are tailored to quantitatively describe changes in the near-surface warming and can only provide a qualitative picture of the changes in those three variables.

|                    | 2 m temperature | 850 hPa zonal wind | precipitation rate | sea-ice fraction |
|--------------------|-----------------|--------------------|--------------------|------------------|
| 2-PCA variance [%] | 62              | 66                 | 61                 | 79               |
| MLR variance [%]   | 54              | 17                 | 22                 | 23               |

223 **Table 1: Explained variance over the Arctic (poleward of 55° N) for each target variable in the extended boreal summer (May to**  
224 **October), expressed as a percentage of the total variance across model projections. Each column shows a target variable. The first**  
225 **row is the amount of variance explained by the first 2 modes of a PCA on the respective target variable, which is the maximum**  
226 **amount of variance that could be explained by a 2-predictors MLR. The second row is the amount of variance explained by our 2-**  
227 **predictors MLR (Eq. 1), with ArcAmp and BKWarm as predictors.**

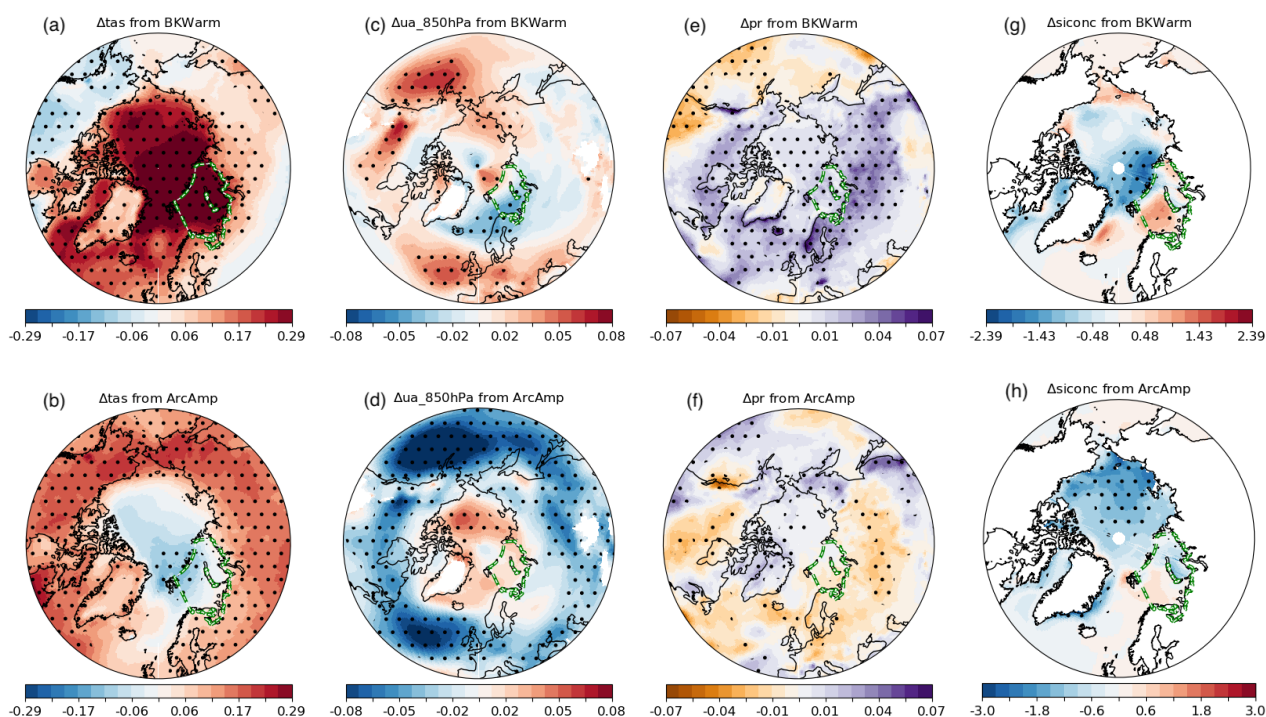
228

229 Figure 2 shows the normalised response of each target variable in the extended summer season to each predictor index, that is  
230 the response per degree of global warming, for a one-standard deviation in the intermodel spread of the predictor index. A  
231 warm anomaly in the Barents-Kara Sea (BKWarm) is associated with the following: a warm anomaly in the 2 m temperature  
232 over the Central (marine) Arctic (Fig. 2a); a dipolar anomaly in the 850 hPa zonal wind changes, with weaker winds over the  
233 Atlantic sector of the Arctic but stronger winds over the Pacific sector (Fig. 2c); positive anomalies in precipitation rates across  
234 all Arctic regions, especially so over land areas (Fig. 2e); and sea-ice loss in the Atlantic sector of the Arctic basin, but with  
235 little influence in the Pacific sector of the Arctic basin (Fig. 2g).

236 These normalised response patterns strongly contrast with that associated with warm anomalies of the lower troposphere in  
237 the Arctic (ArcAmp). For warm anomalies in ArcAmp, we find: 2 m temperature increases over most terrestrial areas (Fig.  
238 2b); the 850 hPa zonal wind weakens over most areas around the Arctic but strengthens in the Central Arctic (Fig. 2d);  
239 precipitation rates are reduced over most high-latitude land areas (Fig. 2f); and sea-ice loss is reduced mostly in the Pacific  
240 sector of the Arctic basin (Fig. 2h). Both 2 m temperature and precipitation rates response to ArcAmp are opposite to that  
241 associated with warm anomalies over the Barents-Kara Sea. This difference in the normalised response to BKWarm and



242 ArcAmp reflects important differences in how our two predictor indices can modulate climate change and explain the diversity  
 243 of model projections found under the SSP5-8.5 scenario forcings.  
 244

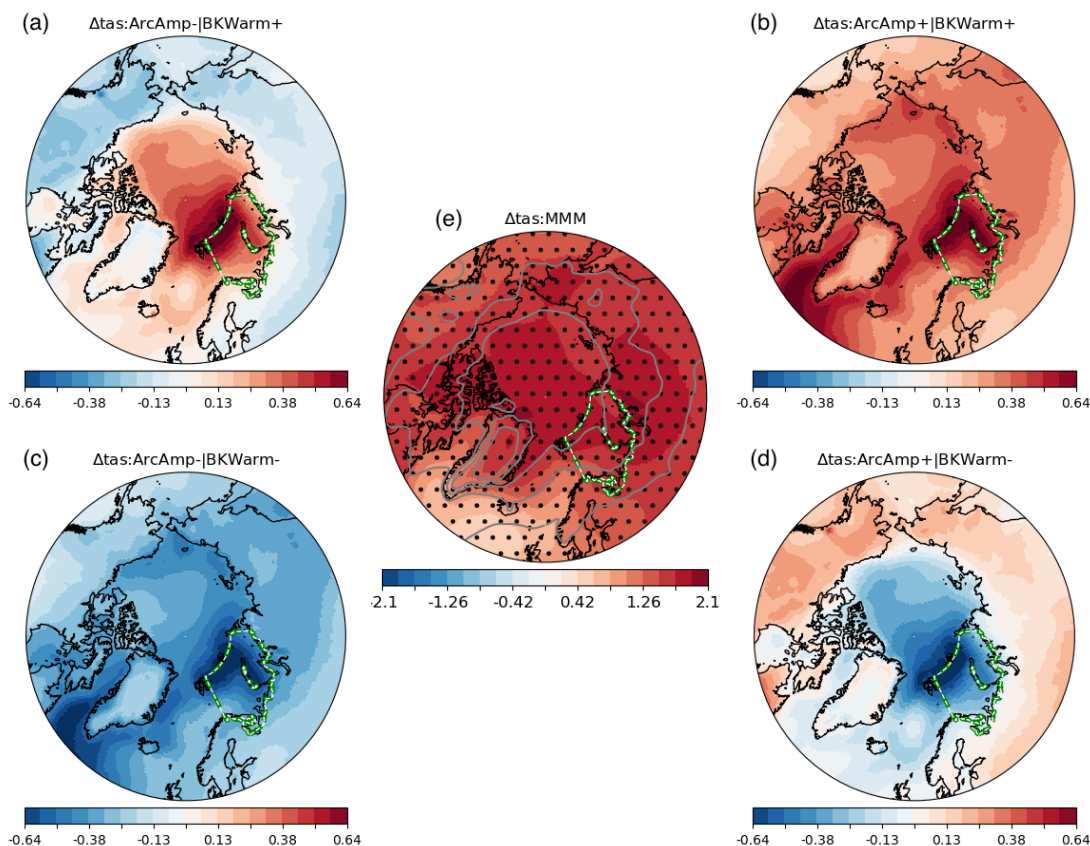


245 **Figure 2: Normalised response of (from left to right) 2 m temperature [K K<sup>-1</sup>], 850 hPa zonal wind [m s<sup>-1</sup> K<sup>-1</sup>], precipitation rate [mm**  
 246 **day<sup>-1</sup> K<sup>-1</sup>], and sea-ice fraction [% K<sup>-1</sup>], to a one-standard deviation in each of the predictor index for BKWarm (top row) and**  
 247 **ArcAmp (bottom row). The normalised response is the product of the regression coefficient  $\beta_i$  in Eq. (1) with  $\sigma_{\Delta\hat{p}_i}$ , a one-standard**  
 248 **deviation anomaly in the associated predictor index. Stippling indicates statistical significance at the 95% confidence level using**  
 249 **Student's t test (i.e., p-value less than 0.05). The green dashed line delineates the outline of the Barents-Kara Sea.**  
 250  
 251

252 Using these normalised responses to each predictor index, we produce four storylines for each of the four target variables  
 253 according to Eq. (3). Specifically, we describe the following four storylines, referenced from A to D and defined in Eq. (3): A:  
 254 ArcAmp- / BKWarm+, B: ArcAmp- / BKWarm-, C: ArcAmp+ / BKWarm+, D: ArcAmp+ / BKWarm-. Figure 3 shows  
 255 the storylines of 2 m temperature change. First, we note that the storylines' patterns are strongly similar to that obtained from  
 256 the two first modes of the PCA on 2 m temperature change (compare Fig. 3a-d with A1a-d); this confirms that our ArcAmp  
 257 and BKWarm predictors capture well the dominant modes of variability that drive the intermodel spread in surface warming  
 258 projections. Consistent with the normalised response patterns (Fig. 2a-b), the main difference in 2 m temperature between the  
 259 four storylines is the rate of warming between marine and terrestrial areas of the Arctic (Fig. 3). In the MMM, the 2 m  
 260 temperature is found to increase by about 1.5 to 2 K K<sup>-1</sup> over most oceanic and terrestrial areas of the Arctic (Fig. 3e), showing



261 a relative uniformity in magnitude across the Arctic. For positive anomalies in both BKWarm and ArcAmp, i.e., storyline B,  
 262 the rate of warming is increased over most Arctic areas (Fig. 3b); the opposite situation is found in storyline C, i.e., negative  
 263 BKWarm and ArcAmp anomalies, with a reduced rate of warming over most Arctic areas (Fig. 3c). For positive (negative)  
 264 anomalies in BKWarm but negative (positive) anomalies in ArcAmp, i.e., storyline A (D), the rate of warming is increased  
 265 (reduced) over marine areas but reduced (increased) over terrestrial areas when compared to the MMM (compare Fig. 3a with  
 266 3d). Changes are stronger over marine areas, especially in the northern part of the Barents-Kara Sea and the Western North  
 267 Atlantic basin, where values can depart by up to 30% compared to the MMM. Out of all four storylines, storylines A and D  
 268 show the largest deviation in warming rates between terrestrial and marine areas (Fig. 3a,d). Beyond an amplification or  
 269 dampening of the MMM climate response, our analysis suggests a decoupling of the near-surface temperature warming  
 270 between terrestrial and marine areas, with the former being associated with the lower-tropospheric warming and the latter  
 271 connected to changes in the Barents-Kara and North Atlantic basin.  
 272



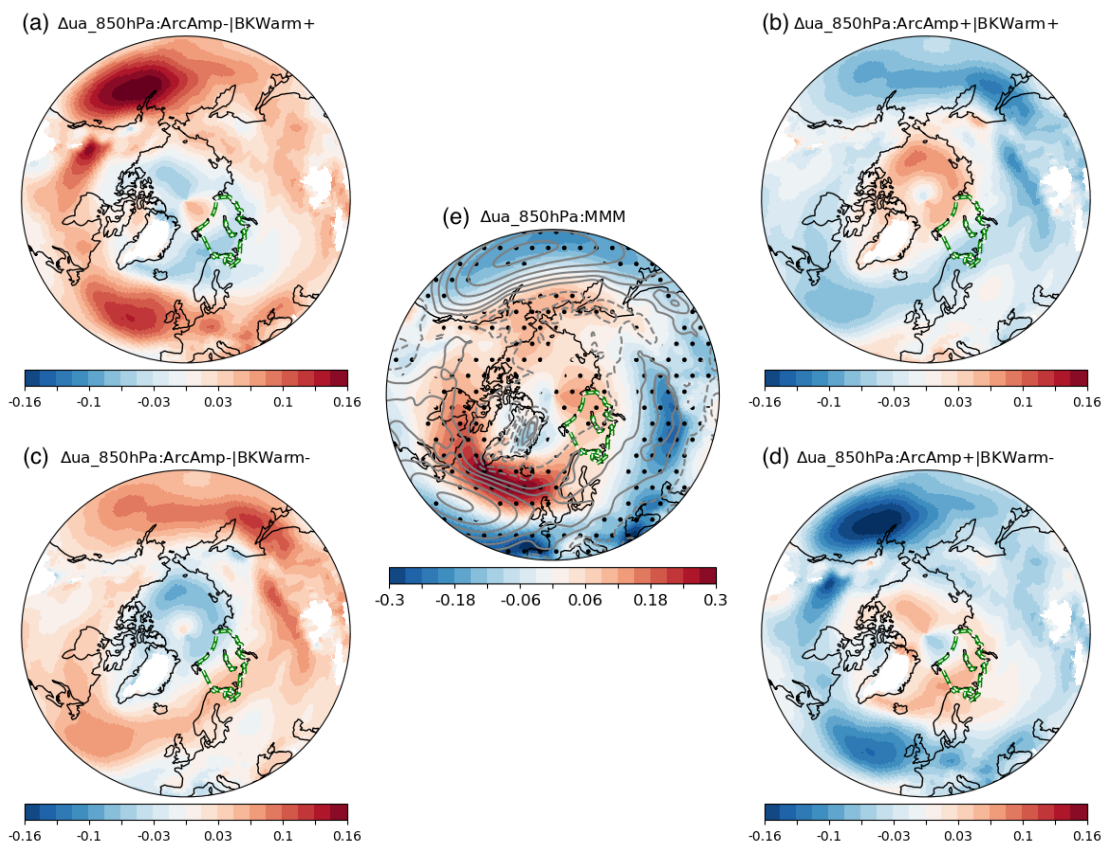
273  
 274 **Figure 3: (a)-(d) Storylines of climate change for 2 m temperature as defined in Eq. (3a-d) and (e) its MMM projection. Units: K K<sup>-1</sup>.**  
 275 **Stippling on (e) indicates areas where at least 80% of the models agree on the sign of change, and grey solid contours indicate the**  
 276 **MMM present-day climatology. The green dashed line delineates the outline of the Barents-Kara Sea.**



277

278 In comparison with the 2 m temperature, changes in the 850 hPa zonal wind show more complexity in the spatial pattern of  
279 changes between the four storylines. In the MMM, change in the 850 hPa zonal wind (U850) shows westerly tendencies across  
280 a wide area in the circumpolar regions, spanning eastward from the Bering Sea to the Barents-Kara Sea, with a maximum over  
281 the North Atlantic between Southern Greenland and Scandinavia. The westerly tendencies extend to the Pacific sector of the  
282 Arctic Ocean, forming an arch stretching from the Beaufort Sea to the Laptev Sea. On the other hand, easterly tendencies are  
283 found in the midlatitude regions of Central Siberia. Overall, those changes suggest that in the MMM, westerly winds shift  
284 poleward and strengthen around the subpolar front and in the Central Arctic, in qualitative agreement with previously noted  
285 changes in the Northern Hemisphere mid- and high-latitude regions (Harvey et al., 2020). Going beyond the multi-model mean  
286 changes, storylines indicate a strong modulation of those changes, with storyline changes being up to 50% of the MMM. As  
287 for the 2 m temperature, storylines of U850 show modulation of the MMM response departing from a simple amplification  
288 response. Storylines B and C show a bipolar pattern (Fig. 4b,c), with easterly (westerly) tendency in the circumpolar regions  
289 but westerly (easterly) tendencies over the Arctic ocean in B (C). Likewise, storylines A and D show an apparent bipolar  
290 pattern in climate response, with changes in the subpolar regions being of opposite signs of that found in the Norwegian and  
291 Barents Sea (Fig. 4a,d). Relative to the multi-model mean changes, the poleward shift in the North Atlantic storm tracks is  
292 influenced by both our predictor indices, hence linking the large uncertainty in its prediction across climate models to the  
293 intermodel spread in BKWarm and ArcAmp. For instance, a strengthening of the 850 hPa zonal wind in the subpolar regions  
294 can occur when the strength of changes in ArcAmp and BKWarm act to either oppose each other (storylines A, Fig. 4a), or  
295 complement each other (storylines C, Fig. 4c). This contrasts with the Beaufort Gyre, which shows an amplification or  
296 dampening only when ArcAmp and BKWarm act in concert with each other (Fig. 4b,c). Even if our storylines account for  
297 only a fraction of the model spread in the 850 hPa zonal wind projections, the different outcomes outlined by our storylines  
298 suggest markedly different impacts of global warming on the low-level winds, with implications for changes in synoptic  
299 storms' tracks and intensity changes.

300



301

302

**Figure 4: Storylines of climate change for the 850 hPa zonal wind (a)-(d) and its MMM projection (e). Units: m s-1 K-1. Same convention as Fig. 3 applies.**

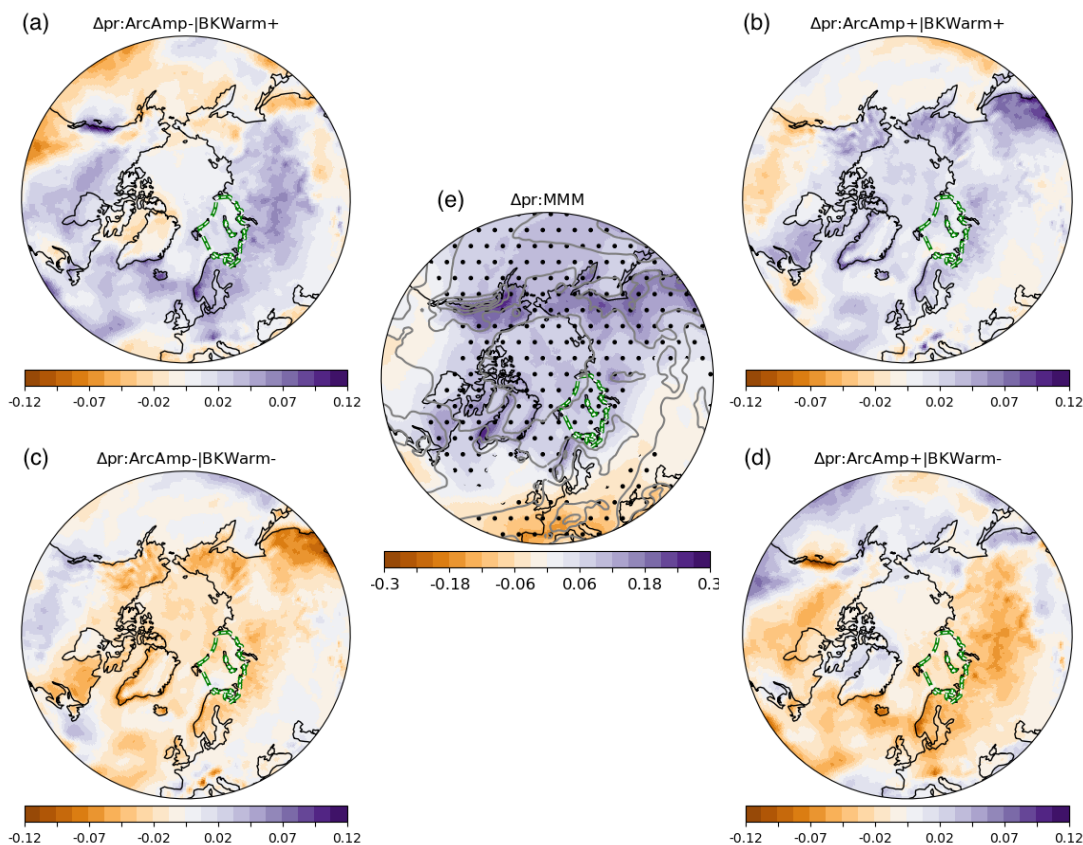
303

304

305

Figure 5 confirms the expected increase in precipitation rate changes in the high-latitude regions, in the MMM. This increase is most pronounced over mountain ranges found on the western sides of continents, which are on the paths of the Atlantic and Pacific storm tracks, e.g., the North American coastal ranges, Western Greenland, Scandinavian coastal ranges (Fig. 5e). This increase in precipitation rate contrasts with the drying tendency found over most of the midlatitude and subtropical regions of Eurasia and North America. Storylines show that projections can differ substantially from this pattern, by up to 50% of the MMM values. In particular, precipitation rate increases over most of the Arctic for positive anomalies in BKWarm (Fig. 5a,b), but decreases for negative anomalies in BKWarm (Fig. 5c,d). Changes over terrestrial areas are generally of greater amplitude than over marine areas across all storylines, and most particularly over regions of strong rainfall in the present-day climate. Overall, storylines of precipitation rates are modulated primarily by change in BKWarm, with only specific regions--notably Greenland and Siberia--showing a response to ArcAmp.

315



316

317

318

319

320

321

322

323

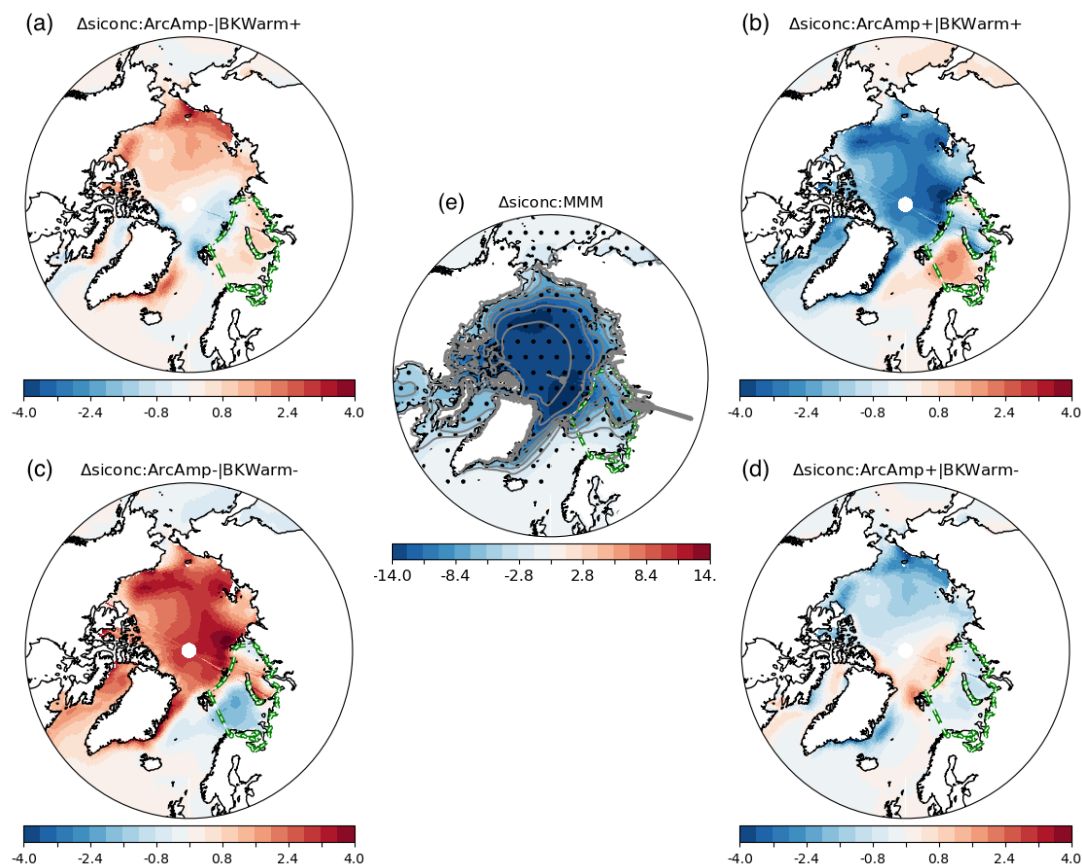
324

325

326

**Figure 5: Storylines of climate change for precipitation (a)-(d) and its MMM projection (e). Same convention as Fig. 3 applies.**

Figure 6 confirms the expected decline in sea-ice across the Arctic in the MMM, with sea-ice fraction displaying loss by at least 15% (cf. Fig. 6e). However, our storylines reveal a more complex picture than suggested by the MMM. On one hand, a pan-Arctic wide amplification/dampening of these changes occur when BKWarm and ArcAmp changes are additive (Fig. 6b,c). On the other hand, large regional contrasts can appear when BKWarm and ArcAmp changes are of opposite sign (Fig. 6a,d): this is especially obvious when comparing the Atlantic and Pacific sector of the Arctic. Those changes appear to be associated largely with the Arctic atmospheric warming, with the Barents-Kara Sea warming playing a more local role with its effect being felt primarily near the Barents-Kara Sea.



327  
328 **Figure 6: Storyline of climate change for sea-ice fraction (a)-(d) and its MMM projection (e).**

#### 329 **4 Discussion and Conclusions**

330 We produced four summertime climate change storylines for the Arctic region, for the four target variables that we consider  
331 to characterise seasonal change in the surface climate: 2 m temperature, precipitation rate, zonal wind at 850 hPa level, and  
332 sea-ice fraction over the Arctic region. We devised those storylines using an established methodology, previously applied to  
333 develop storylines across various midlatitude regions of both hemispheres (ZS17, ML20). We combined this framework with  
334 the realisation that Arctic climate change in summer is tightly associated with two climate indices, the Barents-Kara Sea  
335 warming (BKWarm) and Arctic atmospheric amplification (ArcAmp), which we used as predictors. Our choice of  
336 methodology and predictors was guided by two criteria: (i) our storylines should be representative of the diversity in model  
337 projections, and (ii) our predictors should be connected to physical processes. Criterion (i) ensures that the storylines capture  
338 a meaningful set of possible climate change realisations, while criterion (ii) allows for a scientific understanding of what drives  
339 this diversity in model projections. Criterion (i) is critical to the viewpoint of the end-users who need a plausible range of  
340 climate change scenarios, for instance to develop mitigation strategies, while criterion (ii) is of greater interest to scientists



341 who desire insights regarding the drivers of climate change in the Arctic. When based on those two criteria, storylines can be  
342 used to study possible impacts of climate changes, as well as categorise climate models by storylines; as such storylines are an  
343 efficient way of identifying a few climate models most representative of the diversity of CMIP6 projections.

344  
345 Our storylines are particularly successful at capturing the spread in model projections for the 2 m temperature: our primary  
346 finding is the differential warming rates between terrestrial and marine areas, which we find to be a major source of divergence  
347 in model projections. Our storyline analysis can be applied to other variables, to a varying degree of success: the relevance of  
348 storylines to each target variable must be assessed case-by-case, as different target variables may be controlled by distinct  
349 processes. Likewise, our predictors are less successful at capturing changes in seasons other than the extended boreal summer.  
350 The specificity of storylines to variables, seasons and regions is an important limitation of this methodology, as it relies on  
351 careful tuning to comprehensively represent changes.

352  
353 Using this methodology, we produced the four Arctic climate change: ArcAmp- / BKWarm+ (A), ArcAmp- / BKWarm- (B),  
354 ArcAmp+ / BKWarm+ (C), ArcAmp+ / BKWarm- (D). Our storylines show noticeably different paths for Arctic climate  
355 change, which deviate substantially from the multi-model ensemble mean. Compared to the MMM, cooler surface temperature  
356 in storylines A and C suggests fewer fire risks and less extensive permafrost thawing, if undergoing the same amount of global  
357 warming. Storylines B and D present the opposite outcome, with more intense land warming that may lead to greater fire risks  
358 and more permafrost thawing. Concomitant changes in precipitation rates and surface wind are expected to modulate those  
359 trends: for instance, a wetter summer could imply a reduced fire risk in storyline B compared to D, even if both storylines  
360 show similar rates of warming over land. The combined impacts of physical changes at the surface on climate risks such as  
361 fires and permafrost thaw can only be evaluated with a quantitative analysis that is beyond the scope of our study. Furthermore,  
362 our analysis also shows that enhanced risks over land may or may not translate into enhanced impacts over marine areas. For  
363 instance, storyline A--which showed a lessening of climate risks over land--is tied to an enhanced warming of the Arctic  
364 Ocean and an amplified loss in sea-ice cover, suggesting a more navigable Arctic Ocean and greater disruptions in marine  
365 primary production compared to the MMM. Beyond changes that may be consistent across the entire Arctic, storylines also  
366 suggest futures in which regional contrasts are enhanced. For instance, storylines A and D show sea-ice cover shrinking may  
367 have pronounced differences between the Pacific and Atlantic sectors of the Arctic Ocean; such changes would likely entail  
368 regional differences in the volume of Arctic shipping or marine primary production. Overall, we demonstrate that storylines  
369 can be used to better understand the range of possible climate outcomes for the Arctic that emerge from coupled climate  
370 models, a critical step toward planning for climate mitigation strategies.



## 371 **Appendix A: Empirical storylines**

372 We also tested an empirical method for producing storylines, in which predictor indices emerge from a principal component  
373 analysis (PCA). This is achieved by finding the first two components of a PCA applied to each target variable (von Storch and  
374 Zwiers, 2002), and using those as predictors. Specifically, we can express changes in a target variable  $\Delta Z$  as:

$$375 \Delta Z(x, m) = \overline{\Delta Z}(x) + \sum_{i=1}^N EOF_i(x) PC_i(m) \quad (A1)$$

376 Here,  $EOF_i$  is the eigenmode and  $PC_i$  the eigenvalues of the  $i$ -th mode, and the summation is done over  $N$  principal  
377 components. As in the MLR storylines (Eq. 1), the PCA storylines describe the inter-model variability in model projections,  
378 that is with respect to the MMM changes. Comparing the two frameworks, we find that eigenmode  $EOF_i(x)$  in Eq. (A1) is  
379 analogue to coefficient  $\beta_i(x)$  in Eq. (1), and  $PC_i(m)$  in Eq. (A1) to climate predictor  $\Delta \hat{P}_i(m)$  in Eq. (1). Following the same  
380 methodology to the physical storylines, we produce four “empirical” storylines:

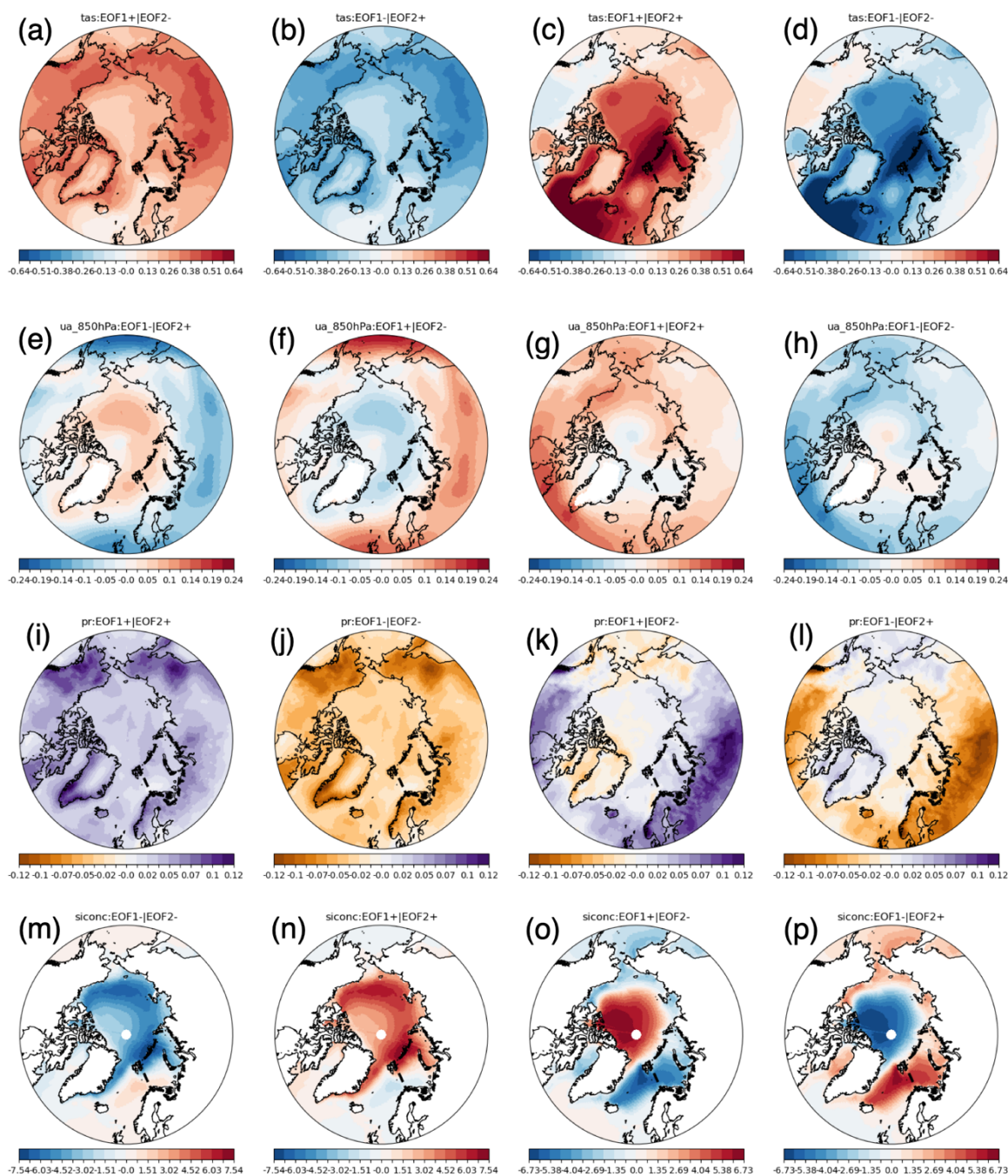
$$381 \widehat{\Delta Z}_{+,+} = s(+EOF_1(x) + EOF_2(x)) \quad (A2a)$$

$$382 \widehat{\Delta Z}_{+,-} = s(+EOF_1(x) - EOF_2(x)) \quad (A2b)$$

$$383 \widehat{\Delta Z}_{-,+} = s(-EOF_1(x) + EOF_2(x)) \quad (A2c)$$

$$384 \widehat{\Delta Z}_{-,-} = s(-EOF_1(x) - EOF_2(x)) \quad (A2d)$$

385 As in Eq. (3),  $s$  defines the standardised climate response in Eq. (A2), which is derived from a Chi-square distribution for 2  
386 degrees of freedom and evaluated on the edge of the 80% confidence boundary region ( $s = 1.26$ ). Compared to the 2-predictors  
387 MLR storylines (Eq. 3), the 2-components PCA storylines (Eq. A2) will better discriminate the spread in model projections,  
388 since the variance explained by the first two components of a PCA maximises the variance that can be explained in the  
389 intermodel spread from any two predictors. While PCA predictors present the advantage of being strictly orthogonal to each  
390 other by construction, they are not directly relatable to specific climate indices or physical processes, which is a substantial  
391 drawback for interpreting changes.



394  
 395 **Figure A1: EOF Storyline of climate change for: 2 m temperature, 850 hPa zonal wind, precipitation, and sea-ice**  
 396 **fraction.**  
 397



398 Empirical storylines show qualitative similarities with the storylines presented in our study (see Fig. A1) to those found in our  
399 physical storylines for most target variables (Fig. 3-6), even if physical storylines consistently underperform empirical ones  
400 with regards to the amount of explained variance in model projections. This is particularly true for the 2 m temperature, which  
401 shows very similar patterns between empirical storylines and our storylines (compare Fig. A1 and 3).

#### 402 **Code availability**

403 The code to generate our Arctic storylines can be found on the first author's GitHub page  
404 ([https://github.com/xlevine/Storylines\\_Analysis\\_ESD](https://github.com/xlevine/Storylines_Analysis_ESD)).

#### 405 **Data availability**

406 This study was based on World Climate Research Programme (WCRP)'s CMIP6 archived simulations, which can be found  
407 on The Earth System Grid Federation (ESGF). This data was stored locally on the National Infrastructure for Research Data  
408 (NIRD), a component of the Norwegian research infrastructure services (NRIS).

#### 409 **Author contribution:**

410 XL performed the formal analysis and was responsible for the data presentation, supervised efforts leading to this work, and  
411 was responsible for the preparation of the manuscript. XL, RW, GM, AO, LG, DH were instrumental in setting the main goals  
412 and structure of this study and setting the storyline methodology. NJ, HL, LN provided important methodological inputs related  
413 to storylines' impact. RW, GM, AO, LG, DH, AK, RK, RW, NJ, HL, LN, PM helped with the preparation of this draft,  
414 providing critical comments. PM procured funding necessary to conduct this study and set the overarching goals of the  
415 PolarRES project that led to this study.

#### 416 **Competing interests:**

417 The authors declare that they have no conflict of interest.

#### 418 **Acknowledgements:**

419 We acknowledge the support of PolarRES (grant number 101003590), a project of the European Union's Horizon 2020  
420 research and innovation programme. Storage and computing resources necessary to conduct this analysis was provided by  
421 Sigma2 — the National Infrastructure for High Performance Computing and Data Storage in Norway (project NS8002K and



422 NN8002K). The CMIP6 simulations used for this analysis were obtained from the Earth System Grid Federation (ESGF), an  
423 infrastructure supported by the World Climate Research Programme (WCRP).

## 424 **References**

425 Anisimov, O.A., and Nelson, F.E.: Permafrost zonation and climate change in the northern hemisphere: results from transient  
426 general circulation models, *Climatic Change*, 35, 241-258, 1997.

427 Arrigo, K.R., and van Dijken, G.L.: Continued increases in Arctic Ocean primary production, *Prog. Oceanogr.*, 136, 60-70,  
428 2015.

429 Callaghan, T.V., Johansson, M., Brown, R.D., Groisman, P.Y., Labba, N., Radionov, V., Barry, R.G., Bulygina, O.N., Essery,  
430 R.L., Frolov, D.M., and Golubev, V.N.: The changing face of Arctic snow cover: A synthesis of observed and projected  
431 changes, *Ambio*, 40, 17-31, 2011.

432  
433 Chadburn, S.E., Burke, E.J., Cox, P.M., Friedlingstein, P., Hugelius, G., and Westermann, S.: An observation-based constraint  
434 on permafrost loss as a function of global warming, *Nature Clim. Change*, 7, 340–344, 2017.

435 Cinquini, L., Crichton, D., Mattmann, C., Harney, J., Shipman, G., Wang, F., Ananthakrishnan, R., Miller, N., Denvil, S.,  
436 Morgan, M., and Pobre, Z.: The Earth System Grid Federation: An open infrastructure for access to distributed geospatial data,  
437 *Future Gener. Comp. Sy.*, 36, 400-417, 2014.

438 Cohen, J., Screen, J.A., Furtado, J.C., Barlow, M., Whittleston, D., Coumou, D., Francis, J., Dethloff, K., Entekhabi, D.,  
439 Overland, J, and Jones, J.: Recent Arctic amplification and extreme mid-latitude weather, *Nature Geosci.*, 7, 627–637, 2014.

440  
441 Dai A., Luo D., Song M., and Liu J.: Arctic amplification is caused by sea-ice loss under increasing CO<sub>2</sub>. *Nat Commun.*, 10,  
442 121, 2019.

443 Dowdy, A.J., Mills, G.A., Finkele, K., and de Groot, W.: Index sensitivity analysis applied to the Canadian forest fire weather  
444 index and the McArthur forest fire danger index, *Meteorol. Appl.*, 17, 298-312, 2010.

445 England, M.R., Eisenman, I., Lutsko, N.J., and Wagner, T.J.W.: The recent emergence of Arctic Amplification, *Geophys. Res.*  
446 *Lett.*, 48, e2021GL094086, 2021.

447 Eyring, V., Bony, S., Meehl, G.A., Senior, C.A., Stevens, B., Stouffer, R.J., and Taylor, K.E.: Overview of the Coupled Model  
448 Intercomparison Project Phase 6 (CMIP6) experimental design and organization, *Geosci. Model Dev.*, 9, 1937-1958, 2016.

449 Harvey, B.J., Cook, P., Shaffrey, L.C., and Schiemann, R.: The response of the northern hemisphere storm tracks and jet  
450 streams to climate change in the CMIP3, CMIP5, and CMIP6 climate models, *J. Geophys. Res.-Atmos.*, 125,  
451 p.e2020JD032701, 2020.



- 452
- 453 Hawkins, E., and Sutton, R.: The potential to narrow uncertainty in regional climate predictions, *B Am. Meteorol. Soc.*, 90,  
454 1095–1108, 2009.
- 455 Hjort, J., Streletskiy, D., Doré, G., Wu, Q., Bjella, K., and Luoto, M.: Impacts of permafrost degradation on infrastructure,  
456 *Nat. Rev. Earth Environ.*, 3, 24–38, 2022.
- 457 Ingvaldsen, R.B., Assmann, K.M., Primicerio, R., Fossheim, M., Polyakov, I.V. and Dolgov, A.V.: Physical manifestations  
458 and ecological implications of Arctic Atlantification, *Nat. Rev. Earth Environ.*, 2, 874–889, 2021.
- 459 Arias, P., Bellouin, N., Coppola, E., Jones, R., Krinner, G., Marotzke, J., Naik, V., Palmer, M., Plattner, G.K., Rogelj, J. and  
460 Rojas, M. (Eds): *Climate Change 2021: the physical science basis, Contribution of Working Group I to the Sixth Assessment  
461 Report of the Intergovernmental Panel on Climate Change, 2021.*
- 462
- 463 Jansen, E, Christensen, J.H., Dokken, T., Nisancioglu, K.H., Vinther, B.M., Capron, E., Guo, C., Jensen, M.F., Langen, P.L.,  
464 Pedersen, R.A., and Yang, S.: Past perspectives on the present era of abrupt Arctic climate change, *Nature Clim. Change*. 10,  
465 714–721, 2020.
- 466
- 467 Jenkins, M., and Dai, A.: The impact of sea-ice loss on Arctic climate feedbacks and their role for Arctic amplification,  
468 *Geophys. Res. Lett.*, 48, e2021GL094599, 2021.
- 469
- 470 Jung, O., Sung, M.K., Sato, K., Lim, Y.K., Kim, S.J., Baek, E.H., Jeong, J.H., and Kim, B.M.: How does the SST variability  
471 over the western North Atlantic Ocean control Arctic warming over the Barents–Kara Seas?, *Environ. Res. Lett.*, 12, 03402,  
472 2017.
- 473 Krikken, F., Lehner, F., Haustein, K., Drobyshev, I., and van Oldenborgh, G. J.: Attribution of the role of climate change in  
474 the forest fires in Sweden 2018, *Nat. Hazards Earth Syst. Sci.*, 21, 2169–2179, 2019.
- 475 Lee, H., Johnston, N., Nieradzik, L., Orr, A., Mottram, R.H., van de Berg, W.J., and Mooney, P.A.: Toward Effective  
476 Collaborations between Regional Climate Modeling and Impacts-Relevant Modeling Studies in Polar Regions, *B Am.  
477 Meteorol. Soc.*, 103, E1866–E1874, 2022.
- 478
- 479 Li, M., Luo, D., Simmonds, I., Dai, A., Zhong, L., and Yao, Y.: Anchoring of atmospheric teleconnection patterns by Arctic  
480 Sea ice loss and its link to winter cold anomalies in East Asia, *Int. J. Climatol.*, 41, 547–558, 2021.
- 481 Lind, S., Ingvaldsen, R.B., and Furevik, T.: Arctic warming hotspot in the northern Barents Sea linked to declining sea-ice  
482 import, *Nature Clim. Change*, 8, 634–639, 2018.
- 483



- 484 Masrur, A., Petrov, A.N., and DeGroot, J.: Circumpolar spatio-temporal patterns and contributing climatic factors of wildfire  
485 activity in the Arctic tundra from 2001–2015, *Environ. Res. Lett.*, 13, 014019, 2018.  
486
- 487 McCarty, J.L., Aalto, J., Paunu, V.-V., Arnold, S.R., Eckhardt, S., Klimont, Z., Fain, J.J., Evangelidou, N., Venäläinen, A.,  
488 Tchebakova, N.M., Parfenova, E.I., Kupiainen, K., Soja, A.J., Huang, L., and Wilson, S.: Reviews and syntheses: Arctic fire  
489 regimes and emissions in the 21st century, *Biogeosciences*, 18, 5053–5083, 2021.  
490
- 491 McCrystall, M.R., Stroeve, J., Serreze, M., Forbes, B.C., and Screen, J.A.: New climate models reveal faster and larger  
492 increases in Arctic precipitation than previously projected, *Nat Commun.*, 12, 6765, 2021.
- 493 Meinshausen, M., Nicholls, Z.R., Lewis, J., Gidden, M.J., Vogel, E., Freund, M., Beyerle, U., Gessner, C., Nauels, A., Bauer,  
494 N., and Canadell, J.G.: The shared socio-economic pathway (SSP) greenhouse gas concentrations and their extensions to 2500,  
495 *Geosci. Model Dev.*, 13, 3571–3605, 2020.
- 496 Melia, N., Haines, K., and Hawkins, E.: Sea ice decline and 21st century trans-Arctic shipping routes, *Geophys. Res. Lett.*, 43,  
497 9720–9728, 2016.
- 498 Merlis, T.M., and Henry, M., 2018. Simple estimates of polar amplification in moist diffusive energy balance models, *J.*  
499 *Climate*, 31, 5811–5824, 2018.
- 500 Mindlin, J., Shepherd, T.G., Vera, C.S., Osman, M., Zappa, G., Lee, R.W., and Hodges, K.I.: Storyline description of Southern  
501 Hemisphere midlatitude circulation and precipitation response to greenhouse gas forcing, *Clim. Dynam.*, 54, 4399–4421, 2020.
- 502 Notz, D., and Community S.I.M.I.P.: Arctic sea ice in CMIP6, *Geophys. Res. Lett.* 47, e2019GL086749, 2020.  
503
- 504 O'Neill, B.C., Tebaldi, C., Van Vuuren, D.P., Eyring, V., Friedlingstein, P., Hurtt, G., Knutti, R., Kriegler, E., Lamarque, J.F.,  
505 Lowe, J., and Meehl, G.A.: The scenario model intercomparison project (ScenarioMIP) for CMIP6, *Geosci. Model Dev.*, 9,  
506 3461–3482, 2016.  
507
- 508 Overland, J., Dunlea, E., Box, J.E., Corell, R., Forsius, M., Kattsov, V., Olsen, M.S., Pawlak, J., Reiersen, L.O., and Wang,  
509 M.: The urgency of Arctic change, *Polar Sci.*, 21, 6–13, 2019.
- 510 Pabi, S., van Dijken, G.L., and Arrigo, K.R.: Primary production in the Arctic Ocean, 1998–2006, *J. Geophys. Res.- Oceans*,  
511 113, 2008.
- 512 Peings, Y., Davini, P., and Magnusdottir, G.: Impact of Ural Blocking on Early Winter Climate Variability Under Different  
513 Barents-Kara Sea Ice Conditions, *J. Geophys. Res.-Atmos.*, 128, p.e2022JD036994, 2023.
- 514 Pithan, F., and Mauritsen, T.: Arctic amplification dominated by temperature feedbacks in contemporary climate models,  
515 *Nature Geosci.*, 7, 181–184, 2014.



- 516  
517 Previdi, M., Janoski, T.P., Chiodo, G., Smith, K.L., and Polvani, L.M.: Arctic amplification: A rapid response to radiative  
518 forcing, *Geophys. Res. Lett.* 47, p.e2020GL089933, 2020.
- 519  
520 Previdi, M., Smith, K.L. and Polvani, L.M.: Arctic amplification of climate change: a review of underlying mechanisms,  
521 *Environ. Res. Lett.*, 16, 093003, 2021.
- 522  
523 Rantanen, M., Karpechko, A.Y., Lipponen, A., Nordling, K., Hyvärinen, O., Ruosteenoja, K., Vihma, T., and Laaksonen, A.:  
524 The Arctic has warmed nearly four times faster than the globe since 1979, *Commun. Earth Environ.*, 3, 168, 2022.
- 525  
526 Rignot, E., Velicogna, I., van den Broeke, M.R., Monaghan, A., and Lenaerts, J.T.M.: Acceleration of the contribution of the  
527 Greenland and Antarctic ice sheets to sea level rise, *Geophys. Res. Lett.*, 38, L05503, doi:10.1029/2011GL046583, 2011.
- 528  
529 Russotto, R.D., and Biasutti, M.: Polar amplification as an inherent response of a circulating atmosphere: Results from the  
530 TRACMIP aquaplanets, *Geophys. Res. Lett.*, 47, p.e2019GL086771, 2020.
- 531  
532 Screen, J., and Simmonds, I.: The central role of diminishing sea ice in recent Arctic temperature amplification, *Nature*, 464,  
533 1334–1337, 2010.
- 534  
535 Shepherd, T.G., Boyd, E., Cabel, R.A., Chapman, S.C., Dessai, S., Dima-West, I.M., Fowler, H.J., James, R., Maraun, D.,  
536 Martius, O., and Senior, C.A.: Storylines: an alternative approach to representing uncertainty in physical aspects of climate  
537 change, *Climatic Change*, 151, 555-571, 2018.
- 538  
539 Smedsrud, L.H., Esau, I., Ingvaldsen, R.B., Eldevik, T., Haugan, P.M., Li, C., Lien, V.S., Olsen, A., Omar, A.M., Otterå, O.H.,  
and Risebrobakken, B.: The role of the Barents Sea in the Arctic climate system, *Rev. Geophys.*, 51, 415-449, 2013.
- 540  
541 The IMBIE Team: Mass balance of the Greenland Ice Sheet from 1992 to 2018, *Nature*, 579, 233–239, 2020.
- 542  
543 van den Broeke, M. R., Enderlin, E. M., Howat, I. M., Kuipers Munneke, P., Noël, B. P. Y., van de Berg, W. J., van Meijgaard,  
544 E., and Wouters, B.: On the recent contribution of the Greenland ice sheet to sea level change. *Cryosphere*, 10, 1933–1946
- 545  
546 Von Storch, H. and Zwiers, F.W. (Eds): *Statistical analysis in climate research*. Cambridge University Press, Cambridge,  
547 United Kingdom, ISBN 0511010184, 484 pp., 2002.
- 548  
549 Veraverbeke, S., Rogers, B.M., Goulden, M.L., Jandt, R.R., Miller, C.E., Wiggins, E.B., and Randerson, J.T.: Lightning as a  
550 major driver of recent large fire years in North American boreal forests, *Nature Clim. Change*, 7, 529-534, 2017.



- 551
- 552 Yumashev, D., Hope, C., Schaefer, K., Riemann-Campe, K., Iglesias-Suarez, F., Jafarov, E., Burke, E.J., Young, P.J.,  
553 Elshorbany, Y. and Whiteman, G.: Climate policy implications of nonlinear decline of Arctic land permafrost and other  
554 cryosphere elements, *Nat Commun.*, 10, 1900, 2019.
- 555 Warner, J.L., Screen, J.A., and Scaife, A.A.: Links between Barents-Kara sea ice and the extratropical atmospheric circulation  
556 explained by internal variability and tropical forcing, *Geophys. Res. Lett.*, 47, p.e2019GL085679, 2020.
- 557 Zappa, G., and Shepherd, T.G.: Storylines of atmospheric circulation change for European regional climate impact assessment,  
558 *J. Climate*, 30, 6561-6577, 2017.